Checkpoint signaling abrogation after cell cycle reentry reveals that differentiated neurons are mitotic cells

Chaska C Walton[1], Wei Zhang[1], Iris Patiño-Parrado[1], Estíbaliz Barrio-Alonso[1], Juan-José Garrido[1], José M Frade[1]*

Affiliations:

[1]Department of Molecular, Cellular and Developmental Neurobiology, Cajal Institute (CSIC), Madrid, 28002, Spain.

*Correspondence to: frade@cajal.csic.es

SUMMARY

Mitotic activity associated to neuron cell-death instead of cell-division is reported in neurodegenerative diseases. However, why mitotic activity can take place in supposedly postmitotic neurons and how it is associated to cell-death remains largely unexplained. To address these questions, we have studied the response of primary neurons to oncogenic deregulation using a fusion protein based on truncated Cyclin E and Cdk2. Oncogenic Cyclin E/Cdk2 elicits mitotic checkpoint signaling, resulting in cell-cycle arrest and cell-death. However, as in mitotic cells, checkpoint suppression enables oncogenic cell-cycle progression and neuronal division. Further, neurons actively adapt to the cell-cycle by losing and reforming the axon initial segment, which integrates synaptic inputs to sustain action potentials. We conclude that neurons are mitotic cells in a reversible quiescent-like state, which is falsely portrayed as irreversible by mitotic checkpoints. In extension, neuronal death in lieu of cell-division reflects oncosuppressive checkpoint signaling.

INTRODUCTION

A central belief in neurobiology is that neurons are not mitotic cells. Despite this, it is not clear what makes neurons qualitatively different from mitotic cells. Thus, the capacity to enter the cell-cycle and undergo cell-division has been shown to be retained in differentiating neurons in knockout (KO) and conditional KO models of negative cell-cycle regulators (Aijoka et al., 2007; Chen et al., 2004; Ferguson et al., 2002; Oshikawa et al., 2013; Xu et al., 2014; Zindy et al., 1999), in immature neurons (Anda

et al., 2016; Ray et al., 1993; Oshikawa et al., 2017), and in mature neurons after undergoing de-differentiation (Friedmann-Morvinski et al., 2012). In contrast, in normally differentiated mature neurons acute induction of cell-cycle re-entry results in cell-death instead of cell-division (Al-Ubaidi et al., 1992; Anda et al., 2016; Feddersen et al., 1992; Kuan et al., 2004; Verdaguer et al., 2002), reflecting that the mitotic limitations of neurons are gradually attained with maturation (Anda et al., 2016). This can explain why aberrant neuronal mitotic activity reported in human pathological conditions such Alzheimer's disease (AD) is associated to cell-death instead of cell-division (Frade and Ovejero-Benito, 2015; Herrup and Yang, 2007; Yang et al., 2001). Thus, we are yet to explain how a postmitotic neuron can undergo mitotic activity throughout maturation and why in mature neurons it is associated to cell-death instead of cell-division. One possibility is that the cell cycle machinery becomes proapoptotic as neurons acquire a mature phenotype (Chatterjee et al., 2016; Greene et al. 2007; Konishi et al., 2002). An alternative explanation is that neurons are mitotic cells in a quiescent-like state that, like standard proliferating cells suffering unscheduled cell-cycle re-entry, can activate cell-cycle checkpoints (Halazonetis et al., 2008; Manic et al., 2015; Musacchio and Salmon, 2007) and undergo cell-death to prevent potentially cancerous cell division (Halazonetis et al., 2008; Vitale et al., 2011). Hence, unscheduled mitotic activity taking place in quiescent mitotic neurons could result in cell-death instead of cell-division by eliciting checkpoint activation.

Cyclin E is necessary for cell-cycle re-entry from quiescence (Geng et al., 2003) and it is expressed in the brain to levels comparable to organs with proliferating cells (Odajima et al., 2011). In cycling mitotic cells, Cyclin E is the canonical late G1 cyclin that triggers transition into S-phase by activating Cyclin-dependent kinase 2 (Cdk2) (Siu et al., 2012). Further, Cyclin E deregulation is oncogenic (Siu et al., 2012). Thus, Cyclin

E is likely central in aberrant neuronal cell-cycle re-entry. Along these lines, upregulation of Cyclin E is reported in AD (Hoozemans et al., 2002; Nagy et al., 1997) and in models of aberrant neuronal cell-cycle re-entry in response to amyloid β (Aβ) (Copani et al., 1999; Lee et al., 2017), excitotoxicity induced by glutamate (Veas-Pérez de Tudela et al., 2015) and kainic acid (Verdaguer et al., 2002), Parkin deficiency (Staropoli et al., 2003), treatment with Parkinsonian mimetic 1-Methyl-4-phenylpyridinium (MPP^+) (Harbison et al., 2011), toxic concentrations of hydrogen peroxide (Schwartz et al., 2007), and the overexpression of the AD-associated mir-26b (Absalon et al., 2013). However, it is yet to be determined whether Cyclin E deregulation can induce neuronal cell-cycle re-entry as it does in mitotic cells and whether it has comparable consequences.

Deregulated Cyclin E induces known alterations on the cell-cycle machinery of mitotic cells (Teixeira and Reed, 2017), which affords predictable checkpoint activation if neurons are mitotic cells. In mitotic cells, checkpoints are present in G1, S, G2 and M-phases of the cell-cycle and can be sequentially abrogated to afford progression through these phases and ultimately cell-division (Halazonetis et al., 2008; Lan and Cleveland, 2010; Manic et al., 2015). Thus, we induced neuronal cell-cycle re-entry with an oncogenic low molecular weight (LMW) Cyclin E isoform (Cyclin ET1) (Porter et al., 2001) fused to Cdk2 (t1EK2). This was coupled with checkpoint signaling abrogation in S, G2 and M-phases to enable cell-cycle progression. We also assessed neuronal adaptation to the cell-cycle and viability by monitoring the integrity of the axon initial segment (AIS). We show that neurons reversibly adapt the AIS to the cell-cycle and that the regulation of S, G2 and M phases, including cell-division, is as standard mitotic cells.

RESULTS

t1EK2 induces DNA synthesis and apoptosis in differentiated neurons

Endogenously expressed Cyclin E has been shown to be able to bind and activate Cdk2 (Schmetsdorf et al., 2009). However, under physiological conditions, Cyclin E forms catalytically inactive complexes with Cdk5 to promote synapse maturation (Odajima et al., 2011). Cdk5 is necessary to prevent cell-cycle re-entry (Cicero and Herrup, 2005) and its deregulation is associated to neuron diseases (Su and Tsai, 2011). Thus, to avoid possible interference of Cyclin E with Cdk5 signaling, we generated a t1EK2 fusion product to induce neuronal cell-cycle re-entry. t1EK2 or control LacZ were co-expressed with red fluorescent protein (RFP) to identify transfected neurons (identified by MAP2-specific labeling). We studied cell-cycle re-entry by assessing DNA replication with 5-bromo-2´-deoxyuridine (BrdU) incorporation. This analysis was performed 1, 1.5, 2, and 3 days after transfecting the oncogene in hippocampal neurons maintained for 15 days *in vitro* (DIV), a stage in which synapses have already been developed (Chin et al., 1995).

Transfected control neurons never replicated DNA (n=491) (Figure S1), confirming that neurons in primary culture at these stages of maturation do not spontaneously re-enter the cell-cycle. This is consistent with the gradual loss of mitotic capabilities of neurons with maturation (Anda et al., 2016). In contrast, t1EK2 induced DNA synthesis in neurons (Figure 1a, b). At 1 day post-transfection (dpt) 52.3 ± 4% t1EK2-expressing neurons incorporated BrdU (Figure 1a). This increased at 1.5 dpt to 58.9 ± 4.3% and then declined to 46.8 ± 5.1% at 2 dpt. Neuronal cell-cycle re-entry induced by t1EK2 evidences that, at least downstream of Cyclin E/Cdk2 activation, the regulation of G1/S transition in neurons is shared with mitotic cells. We did not assess BrdU incorporation at 3 dpt due to widespread deterioration of t1EK2-expressing

neurons, which was suggestive of neuronal death. This was not surprising, as Cyclin E is consistently associated to apoptosis during aberrant cell-cycle re-entry in neurons (Absalon et al., 2013; Copani et al., 1999; Lee et al., 2017; Schwartz et al., 2007; Veas-Pérez de Tudela et al., 2015; Verdaguer et al., 2002). Thus, we assessed if t1EK2 was inducing apoptosis by active caspase-3 immunolabeling. The proportion of neurons expressing t1EK2 that were positive for active caspase-3 (34.7 ± 3.9 %) was already significantly higher than control neurons (6.0 ± 1.9 %) at 1.5 dpt ($p < 0.001$, Fisher's exact test) (Figure 1c). As expected, apoptotic neurons displayed pyknotic nuclei (Fig. 1d). Hence, t1EK2 induced DNA synthesis was associated to apoptotic cell-death in neurons.

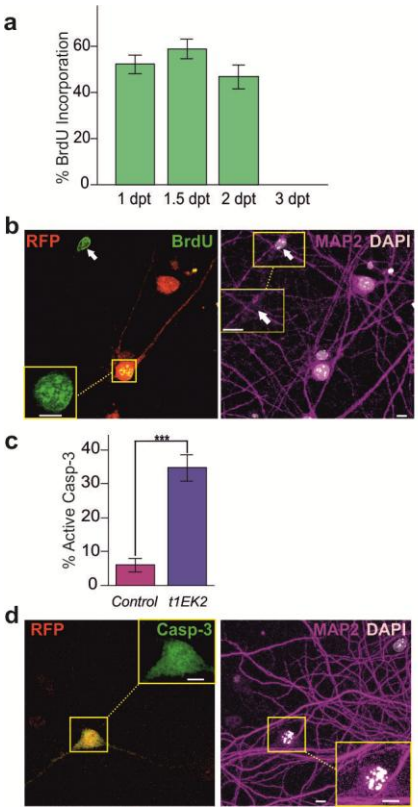

Figure 1. t1EK2 induces DNA synthesis and apoptosis in differentiated neurons. (**a**) BrdU incorporation in t1EK2-expressing neurons at 1, 1.5 and 2 dpt. We did not assess BrdU incorporation at 3 dpt due to widespread neuronal deterioration. (**b**) Confocal images showing BrdU incorporation in t1EK2-expressing neuron. Non-transfected non-neuronal cells (white

arrows) spontaneously incorporate BrdU. (**c**) Percentage of active caspase-3 positive neurons expressing LacZ (Control) or t1EK2 at 1.5 dpt. (**d**) Confocal images of an active caspase-3-positive neuron with pyknotic nucleus. Graphs represent mean percent of RFP/MAP2 neurons positive for BrdU (**a**) or active-Caspase 3 (**c**) and error bars indicate s.e.m. Three independent experiments for **a** (X^2 test of independence and Bonferroni corrected post hoc tests, 1 dpt: n=153, 1.5 dpt: n=129. and 2 dpt: n=94). Three independent experiments for **c** (Fisher's exact test, ***p<0.001, LacZ-expressing Control; n=150, t1EK2: n=150). Scale bar: 12.5 µm.

p53 tumor suppressor dysfunction rescues the neuronal cell-cycle

Oncogenes, and deregulated Cyclin E in particular (Bartkova et al., 2006; Bester et al., 2011; Jones et al., 2013; Neelsen et al., 2013), commonly generate DNA damage that can result in cell death by triggering the DNA damage response (DDR), which is part of the oncosuppressive response of mitotic cells to oncogene-induced cell-cycle re-entry (Halazonetis et al., 2008). Thus, rather than reflecting a postmitotic specific mechanism that elicits cell-death in response to any form of cell-cycle activity, neurons may be responding to t1EK2 by activating standard mitotic oncosuppressive mechanisms. Cancerous cells can escape DDR-elicited apoptotic cell-death by inactivating mutations in tumor suppressor p53 (Halazonetis et al., 2008). Along these lines, p53 loss of function synergizes with oncogenic Cyclin E in carcinogenic processes (Akli et al., 2007; Bagheri-Yarmand et al., 2010; Bartkova et al., 2005; Minella et al., 2002; Smith et al., 2006). Thus, if the regulation of the cell-cycle of neurons is comparable to mitotic cells, a loss of function of p53 should rescue neuronal cell-cycle progression.

To contrast if this was the case, we induced loss of function of p53 by expressing a dominant negative mutant (p53DN) and again assessed apoptosis with active caspase-3. The proportion of active caspase-3 positive t1EK2/p53DN-expressing

neurons (6.0 ± 1.9 %) was not statistically significantly different from control neurons expressing p53DN (1.3 ± 0.9 %) at 1.5 dpt ($p = 0.061$, Fisher's exact test) (Figure 2a). Hence, as in mitotic cells, p53 dysfunction prevented cell-cycle re-entry related cell-death. Moreover, rescued neurons occasionally showed mitotic chromatin condensation (Figure 2b; Movie 1) and could even be rarely be found undergoing possible attempts at cell-division (Figure S2a).

To confirm that preventing cell death also rescued neurons with t1EK2-induced DNA replication, we quantified BrdU incorporation at 1, 2, and 3 dpt. Control neurons never replicated DNA (n=1,045) (Figure S2b). In contrast, inducing p53 loss of function in t1EK2-expressing neurons resulted in sustained BrdU labelling at 1 (38.8 ± 2.5 %), 2 (61.2 ± 2.8 %) and 3 dpt (61.8 ± 3.4 %) (Figure 2c, d). Moreover, neurons with replicated DNA could still be found at 5 dpt (Figure S2c). Thus, in a process that is reminiscent of carcinogenesis in mitotic cells, our results suggest that tumor suppressor loss of function synergizes with t1EK2 to enable neuronal cell-cycle progression.

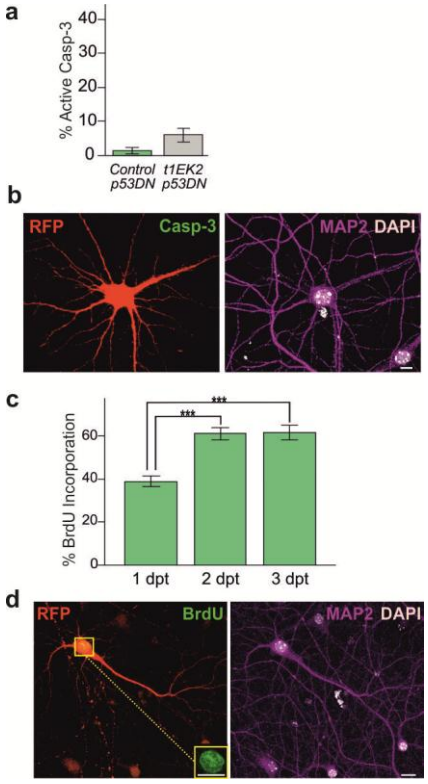

Figure 2. p53 tumor suppressor dysfunction rescues the neuronal cell-cycle. (**a**) Percentage of active caspase-3 positive neurons expressing LacZ/p53DN (Control) or t1EK2/p53DN at 1.5 dpt. (**b**) Confocal image of an active caspase-3-negative neuron presenting mitotic chromatin condensation (for 3D reconstruction of nucleus see Movie 1). (**c**) BrdU incorporation time-course of t1EK2/p53DN-expressing neurons at 1, 2 and 3 dpt. (**d**) Confocal images showing BrdU incorporation in t1EK2/p53DN-expressing neuron. Graphs represent mean percent of RFP/MAP2 neurons positive for active-Caspase 3 (**a**) or BrdU (**c**) and error bars indicate s.e.m. Three independent experiments for **a** (two-sided Fisher's exact test, ***p<0.001, LacZ/p53DN expressing Control; n=150, t1EK2/p53DN: n=150). Three independent experiments for **c** (X^2 test of independence and Bonferroni corrected post hoc tests, ***p<0.001, 1 dpt: n=376, 2 dpt: n=294. and 3 dpt: n=204). Scale bar: 12.5 µm.

Wee1 inhibition enables G2/M transition in differentiated neurons.

To assess cell-cycle progression beyond S-phase, we performed Phospho-Ser10 Histone H3 (pH3) immunostaining to identify neurons in late G2 and M-phase (Hendzel et al., 1997). Consistent with the absence of spontaneous DNA replication, control MAP2-positive neurons were never positive for pH3 (n=150). In contrast, 45.3 ± 4.1% of RFP and MAP2-positive t1EK2/p53DN-expressing neurons reached late G2 (evidenced by pH3-specific foci) (Figure 3a; Figure S3d). Moreover, in fit with active caspase-3-negative neurons occasionally entering M-phase (Figure 2b; Movie 1, Figure S2a), 2.7 ± 1.3% of t1EK2/p53DN-expressing neurons progressed beyond G2 into M-phase (characterized by pan-nuclear pH3 labelling) (Figure 3a; see Figure S3a, b for protocol details). Therefore, although in most cases M-phase entry was blocked, neurons did progress into M-phase.

In mitotic cells, and especially in p53-deficient cells, DNA damage acquired during a genotoxic S-phase can result in G2 checkpoint activation, which blocks M-phase entry (Manic et al., 2015). Cyclin E deregulation results in DNA damage by aberrantly activating the DNA replication machinery (Bartkova et al., 2006; Bester et al., 2011; Jones et al., 2013; Neelsen et al., 2013). Thus, we assessed by Phospho-Ser139 Histone H2AX (γ-H2AX) immunostaining whether the presence of DNA damage in neurons supported a canonical block on M-phase. The proportion of neurons presenting more than 5 γ-H2AX foci was significantly higher in the t1EK2/p53DN-expressing group (78 ± 3.4 %) than in the p53DN-expressing controls (24 ± 3.5 %) at 1.5 dpt ($p < 0.001$, Fisher's exact test) (Figure 3b). Neurons with widespread γ-H2AX staining generally displayed interphase nuclei (Figure 3c left; Movie 2). As in the case of our previous experiments with active caspase-3 (Figure 2b; Movie 1, Figure S2a) and pH3 (Figure 3a), neurons presenting reduced γ-H2AX foci formation could be occasionally found with prophasic-like mitotic chromatin condensation (Figure 3c right;

Movie 2). These results support the possibility that DNA damage in neurons could be blocking M-phase entry by activating the canonical G2 checkpoint.

In mitotic cells, the M-phase block exerted by G2 checkpoint signaling is reversible (Manic et al., 2015). This checkpoint largely relies on Cdk1 inhibitory phosphorylation effected by the Wee1 kinase. Thus, if neurons have standard regulation of G2/M transition, Wee1 inhibition should abrogate G2 checkpoint signaling and afford neuronal M-phase entry. To test this possibility, we abrogated the G2 checkpoint with the Wee1 kinase inhibitor MK1775 (Hirai et al., 2009) and again assessed M-phase entry. Once in M-phase, the loss of pH3 staining begins at anaphase (Hendzel et al., 1997). Hence, we additionally blocked anaphase onset to capture all neurons that entered M-phase (see Figure S3a, c for protocol details). Control MAP2-positive neurons were not found in late G2 or M-phase (n=150). In contrast, 31.3 ± 3.8 % of t1EK2-expressing neurons with p53 dysfunction entered M-phase (Figure 3d). Interestingly, 37.3 ± 3.9 % of neurons were still found in late G2 (Figure 3d). Given the total percentage of neurons positive for pH3 staining was lower without Wee1 inhibition (Figure 3a) than with Wee1 inhibition (Figure 3d), the latter was likely facilitating the progression of remaining neurons in early G2 and S-phase into late G2, in addition to enabling G2/M transition of those already at late G2. In support, the total percentage of neurons in late G2 and M-phase after Wee1 inhibition (Figure 3d) was similar to that of BrdU positive neurons (Figure 2c). As expected, neurons with pan-nuclear pH3 staining showed chromatin condensation characteristic of M-phase (Figure 3e, f; Movie 3). Neuronal M-phase was further confirmed by α-tubulin immunostaining of the mitotic spindle (Figure S3e) and anillin immunolabeling (Figure S3f), which shuttles from the nucleus to the cell cortex during the prophase to prometaphase transition (Piekny and Maddox, 2010).

We observed that neurons in M-phase presented altered dendritic morphology (Movie 3). To gain insights into these alterations, we performed time-lapse experiments. We expressed Histone H2B tagged with EGFP (H2B-GFP) to follow DNA dynamics and the RFP reporter protein to study morphological alterations. In interphase, neurons expressing t1EK2/p53DN generally remained apparently healthy with unaltered gross morphology (Movie 4, left). In contrast, M-phase entry usually involved a loss of RFP reporter signal from dendrites (Movie 4, right), which can reflect a process associated to mitotic cell-rounding.

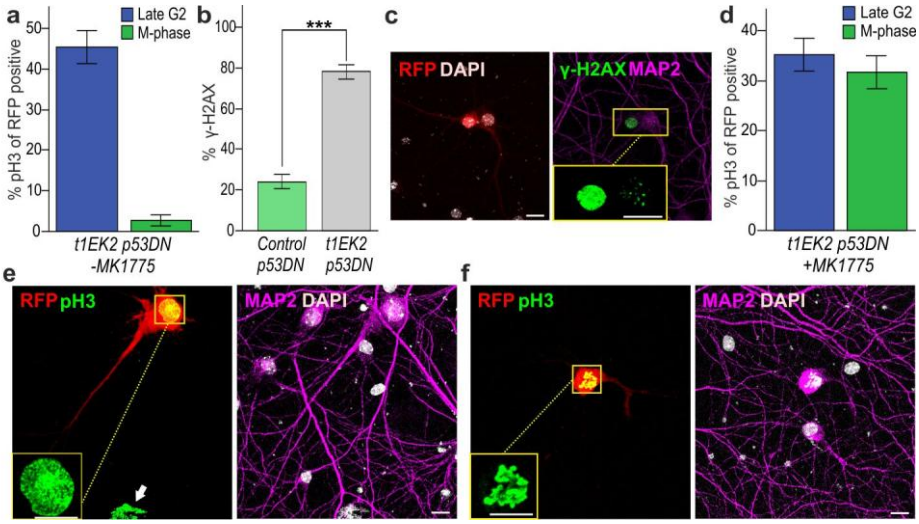

Figure 3. Wee1 inhibition enables G2/M transition in differentiated neurons. (**a**) Percentage of t1EK2/p53DN-expressing neurons with pH3 foci (late G2) or pan-nuclear staining (M-phase) at 1.5 dpt. (**b**) Percentage of t1EK2/p53DN-expressing neurons and control LacZ/p53DN-expressing neurons with more than 5 γ-H2AX foci at 1.5 dpt. (**c**) Confocal image of a neuron with pan-nuclear γ-H2AX staining with interphase nucleus (left) and a neuron with γ-H2AX foci with prophase-like nucleus (right) (for 3D reconstruction of nuclei see Movie 2). (**d**) Percentage of t1EK2/p53DN-expressing neurons at 1.5 dpt in late G2 or in M-phase 3 h after suppressing the G2 checkpoint with MK1775. (**e, f**) Confocal images of a pH3 positive neurons with chromatin condensation consistent with nuclear morphology of prophase (**e**) and

prometaphase (**f**; for 3D reconstruction see Movie 3). White arrow indicates non-neuronal MAP2-negative cell in M-phase (**e**). Graphs represent mean percent of RFP/MAP2 neurons positive for pH3 (**a, d**) or RFP/MAP2 neurons with more than 5 γ-H2AX foci (**b**) and error bars indicate s.e.m. Three independent experiments for **a** (t1EK2/p53DN: n=150). Three independent experiments for **b** (Fisher's exact test, ***p<0.001, LacZ/p53DN expressing Control; n=150, t1EK2/p53DN: n=150). Three independent experiments for **d** (t1EK2/p53DN: n=150). Scale bar: 12.5 µm.

Differentiated neurons undergo cytokinesis

To follow the process of cell-division, we again resorted to time-lapse experiments. After G2 checkpoint abrogation without metaphase arrest, we could not detect t1EK2/p53DN-expressing neurons clearly attempting anaphase or cytokinesis. This could reflect limitations of the neuronal cell-cycle machinery or the effects of t1EK2/p53DN expression itself. The t1EK2 construct used in our experiments is based on a LMW Cyclin E isoform (Porter et al., 2001). These isoforms are reported to induce anaphase/chromatin bridges (Bagheri-Yarmand et al., 2010), which are formed by stretches of DNA that connect chromosomes during anaphase (Fragkos and Naim, 2017). Chromatin bridges can result from unresolved aberrant DNA structures acquired during a deregulated S-phase and lead to cytokinesis failure. Thus, to counter the possible negative effects of a deregulated S-phase on cell-division, we expressed topoisomerase-2α (TOP2α) to aid in the resolution of chromatid intertwines that can underlie some of the aberrant DNA structures in chromatin bridges (Chen et al., 2015) (Figure S4a). Upstream of Wee1, the G2 checkpoint is dependent on ataxia telangiectasia-mutated (ATM) and ataxia telangiectasia and Rad3-related (ATR) to sustain G2 arrest (Manic et al., 2015). Inhibition of ATM/ATR with caffeine results in

G2 checkpoint abrogation (Sarkaria et al., 1999). Thus, we inhibited ATM/ATR upstream of Wee1 with caffeine to induce G2/M transition (see Figure S4a for protocol details). Although still sparse and highly asynchronous, attempts at anaphase/cytokinesis could be detected in 12.9 % (n=93) of recorded neurons. Neurons largely underwent anaphase/cytokinesis failure (n=10) (Movie 5). Despite this, some neurons were able to complete cell-division (n=4), with daughter neurons having independent fates. One of the daughter neurons could die (Figure 4a; Movie 6), or they could both remain viable (Figure 4b; Movie 7). We found that neurons could remain connected by intercellular bridges for hours prior to abscission (Figure 4a; see Figure S4b for protocol details**;** Movie 6), reflecting the presence of persistent chromatin bridges. Alternatively, cytokinesis could also proceed swiftly (Figure 4b; see Figure S4c for protocol details; Movie 7). Therefore, despite t1EK2-induced deregulation, neurons can complete cell-division.

Having ascertained that neurons can complete cell-division, we next assessed markers of telophase and cytokinesis machinery. As seen in time-lapse experiments, neurons did not undergo cell-division synchronously (Figure 4a, b; Movies 6, 7), which challenges its detection by immunocytochemistry. To overcome this limitation, we synchronized anaphase and cytokinesis onset by abrogating the Spindle Assembly Checkpoint (SAC). The SAC delays anaphase onset until the attachment between the kinetochores and the kinetochores fibers of the mitotic spindle are correct (Musacchio and Salmon, 2007). The Monopolar spindle 1 (Mps1) kinase is required to sustain SAC activation until proper attachment (Lan and Cleveland, 2010). Hence, we used the Mps1 inhibitor AZ3146 (Hewitt et al., 2010) to abrogate the SAC and induce synchronous onset of anaphase and cytokinesis (see Figure S4d, e for protocol details). We assessed if neurons were assembling the cytokinesis machinery by anillin immunostaining.

Anillin localizes at the cleavage furrow and remains in the midbody after ingression (Piekny and Maddox, 2010). We found that, as stained by anillin, cleavage furrow ingression began (Fig. 4c) and proceeded asymmetrically (Figure 4d) until the formation of the intercellular bridge/midbody (Figure 4e; Movie 8). To the best of our knowledge, this is the first molecular evidence of the activation of the cytokinesis machinery in neurons. We were also able to detect putative daughter neurons (Figure S4f). Next, we analyzed telophase by pH3 immunolabelling. The loss of pH3 staining begins at anaphase and is completed at telophase (Hendzel et al., 1997). As expected, neurons undergoing cell-division displayed chromatin decondensation that was not stained by pH3, whilst condensed chromatin in intercellular bridges retained pH3 labelling (Figure 4f; Movie 9).

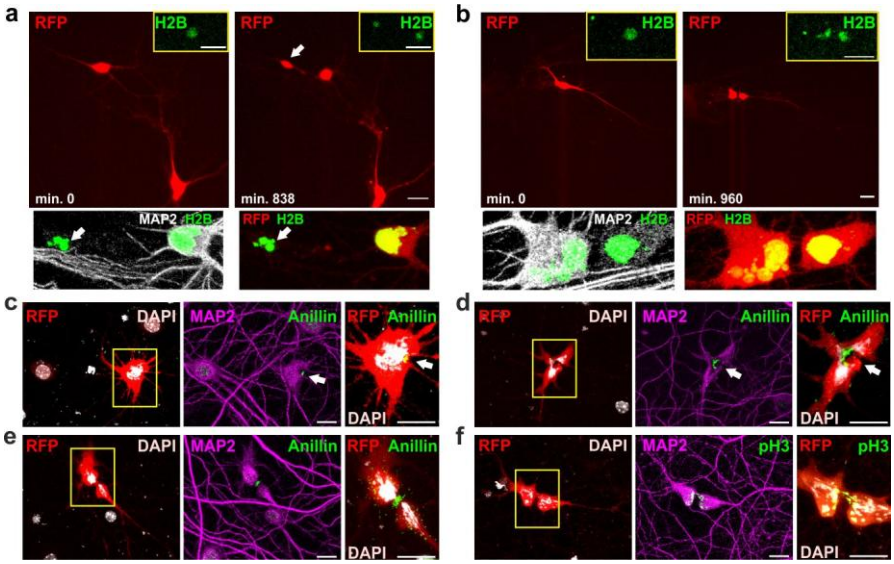

Figure 4. Differentiated neurons undergo cytokinesis. (**a**) Time lapse movie frames of neuron with intercellular bridge delaying abscission (Movie 6). One daughter neuron survived (right) and the other (left) displayed pyknotic nucleus (white arrow). Bottom panels: confocal images of MAP2 immunostaining. (**b**) Time lapse movie frames of neuron in cytokinesis (Movie 7). Bottom panels: confocal images of MAP2 immunostaining. (**c-e**) Confocal images of

anillin immunolabelling of neurons with cleavage furrow ingression (white arrows) at early (c) and late (d) stages, and intercellular bridge/midbody (e, for 3D reconstruction see Movie 8). (**f**) Confocal images of a pH3 positive neuron undergoing cytokinesis (for 3D reconstruction see Movie 9). H2B: Histone H2B tagged with EGFP. Scale bars: 25 µm (a, b, RFP and H2B-EGFP stills), 5 µm (a, b, bottom panels), 12.5 µm (c-f).

Axon initial segment integrity is coordinated with the cell-cycle

Neurons displayed morphological changes upon entry into M-phase (Movies 3-5). These morphological alterations could reflect that neurons actively adapt their biology to enable the cell-cycle. To garner insights into the nature of neuronal adaptations, we assessed changes in the AIS along the cell-cycle. The AIS sustains neuronal polarity and integrates synaptic input to generate action potentials (Rasband, 2010), and previous studies demonstrate that AIS integrity is required to maintain neuronal viability (Schafer et al., 2009). AnkyrinG (AnkG) is the main protein in the AIS and is necessary to maintain AIS functions and neuronal integrity (Rasband, 2010). Thus, we analyzed AnkG immunostaining across different phases within the cell-cycle and after cell-cycle exit (Fig. 5a). However, we did not assess cell-cycle exit after cell-division because daughter neurons displayed signs of aneuploidy (see Fig. 4b, left bottom panel). This would likely confound the analysis of the AIS recovery. Instead, we analyzed multinucleated neurons that exited M-phase without cell-division (Movie 5), as they at least conserve their original genome.

AnkG signal varied significantly across cell-cycle stages [Welch's F test (5, 20.479) = 11.617, $p < 0.001$] (Figure 5a, b), evidencing that AIS integrity fluctuated during the cell-cycle. The AnkG signal of neurons in prophase was not significantly different from that of neurons in interphase ($p = 0.448$) or control transfected neurons (p

= 0.703) (Figure 5a). However, the AnkG signal did decrease significantly in between prometaphase and telophase when compared to interphase (p = 0.003), prophase (p = 0.023) or control neurons (p = 0.009). These results evidence a loss of AIS integrity in M-phase, in between prometaphase and telophase. Six hours after inducing G2/M transition, multinucleated neurons had still not recovered the AnkG signal when compared to interphase (p = 0.033), prophase (p = 0.033) or control neurons (p = 0.041). Hence, the loss of AIS in M-phase was not yet recovered. However, 9 hours after inducing G2/M transition, multinucleated neurons significantly increased their AnkG signal with respect to neurons in between prometaphase and telophase (p = 0.005) and displayed a non-significant tendency when compared to multinucleated neurons fixed 6 hours after inducing G2/M transition (p = 0.065). Further, the AnkG signal was recovered to levels that were not statistically significantly different from control (p = 0.957), interphase (p = 0.999) or prophase (p = 0.349) neurons. Therefore, after cell-cycle exit, neurons progressively yet fully recovered the AIS, a structure that is necessary to sustain action potentials, polarity, and viability (Rasband, 2010, Schafer et al., 2009).

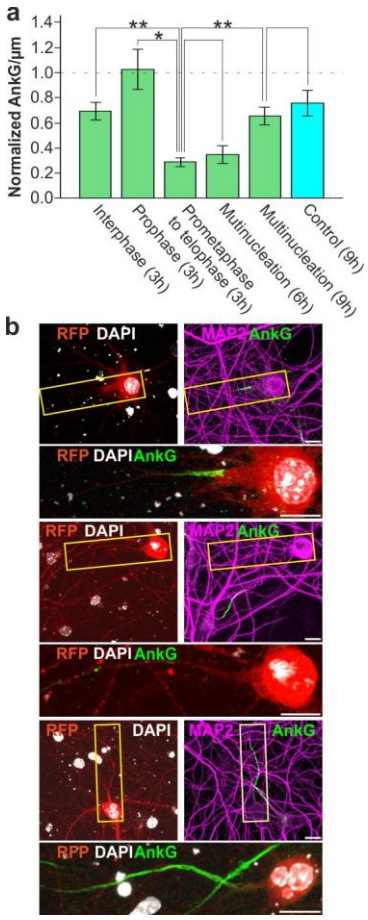

Figure 5. Axon initial segment integrity is coordinated with the cell-cycle. (**a**) Normalized AnkG signal per µm in neurons expressing t1EK2/p53DN/TOP2α (green) in different stages of the cell-cycle, and in control neurons expressing LacZ/p53DN/TOP2α (blue) at the indicated time points after suppressing the G2 checkpoint with MK1775. All groups were treated with AZ3146 to abrogate the SAC 2.5 h after MK1775 treatment. (**b**) Confocal images of AnkG immunolabelled neurons in prophase (top panels), prometaphase to telophase (middle panels), and 9 h multinucleation groups (bottom panels). High magnification of AIS is shown for each case. Scale bar: 12.5 µm. Graphs represent mean AnkG/µm signal of RFP/MAP2 positive neurons normalized to neighboring RFP negative MAP2 positive neurons (**a**) and error bars indicate s.e.m. Single experiment for **a** (Welch's F test and two-sided Games-Howell post-hoc tests, **$p<0.01$, *$p<0.05$, Interphase: n=9, Prophase: n=7, Prometaphase to telophase: n=9, Multinucleation 6 h: n=8, Multinucleation 9 h: n= 10, Control: n = 10).

DISCUSSION

Here we have shown that cell-cycle regulation in mitotic cells and mature neurons is shared. This evidences that the latter are not postmitotic as traditionally considered, but instead they remain mitotically proficient in a reversible quiescent-like state.

The ban on neuronal cell-division

We have induced cell-cycle re-entry with t1EK2, a fusion protein based on Cyclin ET1/Cdk2. Cyclin E/Cdk2 is the holoenzyme that regulates canonical G1/S signaling in mitotic cells (Siu et al., 2012). Thus, t1EK2 induced cell-cycle re-entry evidences that canonical G1/S signaling is present in neurons. Cyclin ET1 is an oncogenic LMW isoform of Cyclin E (Porter et al., 2001). Hence, our results also evidence that neurons are susceptible to oncogenic deregulation. Cyclin E is necessary for cell-cycle re-entry in quiescent cells (Geng et al., 2003) and we show neurons are in a quiescent-like state. Hence, Cyclin E may be a common therapeutic target to prevent mitotic deregulation in diseases such as AD or PD. On the bright side, we have shown that neurons possess functional S, G2 and M-phase machinery and accompanying DDR, G2 checkpoint and SAC signaling to prevents S/G2/M deregulation. Thus, besides being susceptible to oncogene-induced cell cycle re-entry, neurons also possess S, G2 and M-phase oncosuppressive machinery.

Unlike t1EK2-expressing neurons, control neurons never undergo spontaneous cell-cycle re-entry. This is in agreement with the quiescent-like state of neurons under physiological conditions. We suggest that neurons possess “mitotic suppressors” in G0/G1 that prevent physiological cell-cycle re-entry and, consequently, physiological cell-division (Figure S5a). As virtually all Cyclin E expressed in neurons is sequestered

by Cdk5 into inactive Cyclin E/Cdk5 complexes (Odajima et al., 2011), a putative "mitotic suppressor" candidate is catalytically inactive Cdk5. This possibility is supported by previous reports (Cicero and Herrup, 2005). In extension, Cdk5 overactivation, which is associated to neurodegenerative processes (Su and Tsai, 2011), is likely concomitant to the release Cyclin E. Hence, we suggest that pathophysiological events linked to neurotoxic Cdk5 activity can be alternatively or complementarily accounted by Cdk2 activation (Lee et al., 2017). In support, Cdk5 deregulation is associated to aberrant tau phosphorylation (Su and Tsai, 2011) and Cyclin E/Cdk2 can also phosphorylate tau (Schmetsdorf et al., 2009).

Gathering the above, we argue that G0/G1 neuron-specific "mitotic suppressors" prevent physiological neuronal cell-division (Figure S5a) whilst canonical mitotic G1/S/G2/M cell-cycle checkpoints prevent oncogenic-like neuronal cell-division (Figure S5b). As a result, despite neurons are mitotic cells that can undergo cell-division, pathological or physiological neuronal cell-division has never been reported (Frade and Ovejero-Benito, 2015; Herrup and Yang, 2007).

Aberrant cell-cycle activity in neurons and cell-death

If "mitotic suppressors" block physiological cell-cycle re-entry in neurons, cell-cycle activity reported in neuron diseases such as AD or PD (Frade and Ovejero-Benito, 2015; Herrup and Yang, 2007) would invariantly result from oncogenic-like re-entry and, thence, is potentially cancerous in mitotic neurons. As with t1EK2, we suggest that Cdk5 overactivation (Lopes et al., 2009; Veas-Pérez de Tudela et al., 2015), Aβ (Copani et al., 1999, Lee et al., 2017; Lopes et al., 2009), prion proteins (Lopes et al., 2009), MPP^+ (Harbison et al., 2011), DNA damage (Kruman et al., 2004) or excitotoxicity (Staropoli et al., 2003; Veas-Pérez de Tudela et al., 2015; Verdaguer et al., 2002) act as

oncogenes, either directly or indirectly, and, therefore, also require the oncosuppressive block of a potentially cancerous neuronal cell-division. This oncosuppressive block can be achieved by inducing cell-death (Halazonetis et al., 2008; Vitale et al., 2011). In mitotic cells, cell-death can be p53-dependent or independent, apoptotic or necrotic depending on the phase in which cell-death signaling takes place (Halazonetis et al., 2008; Vitale et al., 2011). This can explain why in aberrant neuronal cell-cycle re-entry there are also reports of multiple forms of cell-death (Frade and Ovejero-Benito, 2015; Herrup and Yang, 2007). Therefore, cell-cycle related neuronal cell-death in pathologies such as AD, Parkinson's disease, amyotrophic lateral sclerosis or injury (Frade and Ovejero-Benito, 2015; Herrup and Yang, 2007) may be part of oncosuppressive mechanisms preventing disease progression. Namely successful tumor suppression may entail neurodegeneration in lieu of cancer (Figure S5b).

Aberrant cell-cycle activity in neurons and senescence

Another oncosuppressive response is senescence, which strips mitotic cells from their proliferative capacity and can entail a cytotoxic phenotype (Coppé et al., 2010). As with cell-death, stress induced senescence can be triggered during a deregulated cell-cycle to prevent potentially cancerous cell-division. Unlike cell-death during the cell-cycle, senescence entails exiting the cell-cycle into a viable state. Reports of multinucleated neurons in AD (Zhu et al., 2008) may represent evidence of senescence in AD. Multinucleated cells may have exited the cell-cycle into senescence from M-phase, after aberrant anaphase or failed cytokinesis (Vitale et al., 2011). Our results show that viable multinucleated neurons are produced accordingly. However, most senescence cells are hyperploid mononucleated cells, as they can also result from cell-cycle exit prior to karyokinesis during G1, S, G2 or M-phase (Frade and Ovejero-Benito, 2015; Herrup

and Yang, 2007). Thus, the presence of multinucleated neurons reported in AD (Zhu et al., 2008) would evidence a small fraction of a larger amount of senescent neurons. This alternative phenotype could explain why neurons that have re-entered the cell-cycle in AD largely remain viable for years (Arendt et al., 2010; Herrup and Yang, 2007) and are selectively affected by cell-death throughout disease progression (Arendt et al., 2010). Future work will have to determine whether there is a pathophysiological role for senescence in neuron disease (Fielder et al., 2017). Only models of viable neuronal cell-cycle re-entry can accomplish this aim. To the best of our knowledge, our model with multinucleated neurons is the first of this type.

Regenerative neuronal cell-division

We have shown that differentiated neurons at post-synaptogenesis stages possess functional cell-cycle machinery and can undergo cell-division. Further, AIS dynamics during the cell-cycle and after its premature exit imply that a structural determinant of neuronal viability (Schafer et al., 2009) is coordinated with the cell-cycle. We suggest that, although physiological cell-division is not possible (Figure S5a), controlled abrogation of mitotic suppression can allow for therapeutic physiological-like neuronal cell-division (Figure S5c). Future work will have to determine whether neuronal cell-division can afford therapeutic neuroregeneration. For now, we have established that it is no longer impossible.

METHODS

Plasmids

Construction of a vector encoding a truncated form of Cyclin E (Trunk 1), which lacks the first 39 amino acids of Cyclin E (Porter et al., 2001), fused to Cdk2 isoform 1 (NCBI accession number NP_001789) (t1EK2) was based on the EK2 fusion protein described previously (Jahn et al., 2013). Briefly, a synthetic DNA construct encoding for t1EK2 was firstly cloned into the pUC vector, then subcloned into the HindIII and XbaI sites of pcDNA3 vector (ThermoFisher Scientific) and finally sequence verified. The pcDNA6/V5-His/lacZ vector expressing LacZ was purchased from Invitrogen. The pRFPRNAiC vector expressing red fluorescent protein (RFP), provided by Stuart Wilson (University of Sheffield, UK), has been previously described (Das et al., 2006). The T7-p53DD-pcDNA3 vector expressing a dominant negative form of p53 (Irwin et al., 2000) was a gift from William Kaelin (Addgene plasmid # 25989). The H2B-GFP vector expressing a Histone-GFP fusion protein (Kanda et al., 1998) was a gift from Geoff Wahl (Addgene plasmid #11680). The TOP2α-WT pcDNA3.1(+) vector expressing topoisomerase IIα (Wu et al., 2016) was a kind gift from Corrado Santocanale (National University of Ireland).

Antibodies and inhibitory compounds

Primary antibodies: The anti-BrdU rat monoclonal antibody (mAb) [BU1/75 (ICR1)] (AbDSerotec) was used at 1:200 dilution. The anti-RFP rabbit polyclonal antibody ab62341 (Abcam) was used at 1:100 dilution. The anti-MAP2 chicken antibody ab5392 (Abcam) was diluted 1:5000-1:12000. The cleaved Caspase-3 rabbit antibody (Cell Signaling Technology) was used at 1:400 dilution. The anti-phospho Histone H3 (ser10) rabbit polyclonal antibody 06-570 (Millipore) was used at 1:500 dilution. The anti-anillin rabbit polyclonal antibody ab154337 (Abcam) was used at 1:100 dilution. The anti-α-tubulin mouse monoclonal antibody [DM1A] ab2791 (Abcam) was used at

1:10000 dilution. The anti-phosphoH2AX (ser139) mouse monoclonal antibody [9F3] ab26350 (Abcam) was used at 1:500 dilution. The anti-Ankyrin-G mouse antibody [N106/36] (NeuroMab) was diluted at 1:150. Secondary antibodies: Alexa Fluor 488 Goat Anti-Rat IgG (H+L) (Life Technologies), Alexa Fluor 488 Goat Anti-Mouse IgG (H+L) (Life Technologies), Alexa Fluor 488 Goat anti-Mouse IgG2a A-21131 (Invitrogen), Alexa Fluor 488 Affinipure Goat Anti-Rabbit IgG (H+L) (Jackson Immunoresearch), Alexa Fluor 594 Goat Anti-Rabbit IgG (H+L) (Life Technologies), and Alexa Flour 647 Goat Anti-Chicken IgY (H+L) A-21449 (Invitrogen) were used at 1:1000 dilution. Inhibitors: Cdk1 inhibitor RO3306 (ref. 1530) was used at 9 µM, Wee1 inhibitor MK1775 (ref. 1494), used at 900 nM, and Mps1 inhibitor AZ3146 (ref. 1642), used at 10 µM, were purchased from Axon Medchem. The Eg5 inhibitor monastrol (ab14087), used at 100 µM, and the proteasome inhibitor MG132 (ab141003), used at 10µM, were purchased from Abcam. Caffeine (Sigma), used at 3 mM, was diluted in Neurobasal without L-Glutamine (ThermoFisher Scientific) and filter sterilized with 0.2 µm syringe filters (Acrodisc).

Hippocampal Cultures

10-mm diameter coverslips (Menzel Glässer) were placed in 65% nitric acid (Merck) overnight. Coverslips were then washed 4 times in Milli-Q water (Millipore), once in pure ethanol (Merck) and air-dried. Coverslips were sterilized overnight in oven at 185ºC, placed in CELLSTAR cell culture dishes with 4 inner rings (Greiner bio-one) and UV sterilized for 1 h. Coverslips were coated with 0.5 mg/ml polyornithine (PLO) (Sigma-Aldrich) (prepared in 150 mM borate buffer, pH8.4) for at least 24 h. PLO was washed twice in sterilized Milli-Q water. CELLSTAR culture dishes were left in a humidified atmosphere containing 5 % CO_2 at 37°C with 2ml of neuronal plating

medium consistent of Dulbecco's modified Eagle medium (DMEM) with D-Glucose, L-Glutamine and Pyruvate (ThermoFisher Scientific) containing 10 % fetal bovine serum (FBS) (Life technologies) and penicillin-streptomycin (25 U/ml) (Gibco). Primary hippocampal neurons derived from CD-1 mice (Charles River) were harvested from embryonic day 17, staged as previously described (Kaufman, 1992). Pups were decapitated and brains were placed in cold Hanks' balanced salt solution (HBSS) without calcium chloride, magnesium chloride, nor magnesium sulphate (Gibco). Hippocampi were then dissected and incubated for 15 min at 37ºC in 5 ml HBSS containing 2.5 mg/ml trypsin (Gibco) in a 15 ml conical centrifuge tube. 1 mg/ml DNAse (Roche) was added for the last 30 s. Hippocampi were then washed 5 times in 5 ml of HBSS at 37ºC each time. Mechanical dissociation followed in 1ml of HBSS at 37ºC by passing hippocampi through a Pasteur pipette 10-15 times. Non-dissociated tissue was allowed to collect at the bottom by gravity and clean supernatant with dissociated cells transferred to a new 15 ml centrifuge tube. 1 ml of HBSS at 37ºC was added to the remaining tissue and dissociated again with a flame polished Pasteur pipette to reduce the diameter of the tip 10-15 times. Non-dissociated tissue was allowed to collect at the bottom by gravity. Clean supernatant with dissociated cells was transferred to the same centrifuge tube in which cells from the first dissociation were collected. Neurons were transferred at a density of 24.000 cells/cm^2 to CELLSTAR cell culture dishes (Greiner bio-one) with neuronal plating medium. Neurons were allowed to attach to coverslips for 3 to 4 h in a humidified atmosphere containing 5 % CO_2 at 37°C. Once neurons were settled onto the coverslips, neuronal plating medium was washed with maintenance medium consistent of Neurobasal without L-Glutamine (ThermoFisher Scientific) medium supplemented with B27 (ThermoFisher Scientific), penicillin-streptomycin (25 U/ml) (Gibco) and GlutaMAX (Gibco) and differentiated

with the same medium up to 3-4 DIV. Half of the culture medium was exchanged by fresh maintenance medium without penicillin-streptomycin every 3-4 days.

Lipofection

All lipofections were carried out in hippocampal neurons differentiated for 15 DIV. Two or three days prior to lipofection, half of the culture medium was changed for fresh growth medium without penicillin-streptomycin. In order to increase viability, recovery medium was prepared from conditioned medium of neuronal cultures and used after lipofection. Thus, 30-60 min prior to lipofection, half of the conditioned medium of each neuronal culture (1 ml) was removed and collected into a clean culture dish containing 1 ml of fresh growth medium. BrdU (5 µg/ml) and or inhibitors were added to the recovery medium as needed. The recovery medium was then incubated in a humidified atmosphere containing 5 % CO_2 at 37°C for the duration of the lipofection. Neurobasal medium without supplements pre-warmed to 37°C was added to each of the neuronal cultures. Cultures were returned to the incubator for a minimum of 30 min to stabilize CO_2 levels. To maximize viability, neurons were lipofected in their own culture dish and remaining conditioned medium, which was free of penicillin-streptomycin by 15 DIV. Neurons were transfected with Lipofectamine 2000 (Invitrogen). Lipoplexes were prepared at a ratio of 1 µl of Lipofectamine per 1 µg of DNA. For immunocytochemistry experiments, RFP DNA was always transfected at a 1:20 ratio. Total transfected DNA per culture dish for t1EK2/RFP and LacZ/RFP experiments was 6.4 µg and total transfected DNA per culture dish for t1EK2/p53DN/RFP, LacZ/p53DN/RFP, t1EK2/p53DN/TOP2α/RFP, LacZ/p53DN/TOP2α-RFP experiments was 12.85 µg. For time-lapse experiments, RFP DNA was also transfected at 1:20. Total transfected DNA for t1EK2/p53DN/H2B-EGFP was 10.27 µg and for

t1EK2/p53DN/TOP2α/H2B-EGFP it was 12.44 µg. Lipofectamine was mixed with Neurobasal to a final volume of 250 µl per culture dishand left for 3-5 min. Next, plasmid DNA diluted in 250µl of Neurobasal per culture dish was added and left for 20 min at room temperature. Thereafter, 0.5 ml of the mix was added to each culture dish and left for 90 min. Lipofectamine was then washed out 3 times with 2 ml of growth medium medium pre-warmed to 37ºC. After washout, the recovery medium was added to its corresponding neuronal culture. For cytokinesis experiments, cultures were supplemented with 1xEmbryoMax Nucleosides (Merck) (Bester et al., 2011).

Immunocytochemistry

Hippocampal cultures were fixed for 15 min with 4 % paraformaldehyde (PFA) at RT, and permeabilized for 30 min with phosphate buffered saline (PBS) containing 0.05 % Triton X-100 (Sigma-Aldrich) (0.1% for AnkG staining) (PBTx). For BrdU inmunolabeling, DNA was denatured for 30 min at RT with 2N HCl/0.33× PBS, and then neutralized with three 15-min washes with 0.1 M sodium borate, pH 8.9, and a wash of 5 min with PBTx. Cultures were then incubated for 30 min at RT with PBTx containing 10 % FBS to block antibody unspecific binding, followed by a 1-h incubation at RT with PBTx/1 % FBS and the appropriate primary antibodies. After 4 washes in PBTx, cultures were incubated for 1 h at RT in PBTx containing 1 % FBS and the appropriate secondary antibodies. After 4 additional washes as above, DNA labelling was performed using PBS containg 100 ng/ml 4',6-diamidino-2-phenylindole (DAPI) (Sigma-Aldrich) and the preparations were mounted in glycerol (Panreac)/PBS (1:1).

Image analysis and cell counting studies

For BrdU incorporation time-course experiments, the proportion of BrdU positive neurons out of all MAP2 positive transfected neurons of 10-mm diameter coverslips (MenzelGlässer) was calculated in 3 independent experiments. To assess apoptosis, the proportion of active Caspase-3 (Mazumder et al., 2008) positive neurons of all MAP2 positive transfected neurons was calculated in each of 3 independent experiments. DNA damage was assessed with Phospho-Ser139 Histone H2AX (γ-H2AX) (Kinner et al., 2008). The proportion of neurons with more than 5 γ-H2AX foci or γ-H2AX pan-nuclear staining out of all MAP2 positive transfected neurons was calculated in each of 3 independent experiments. Phospho-Ser10 Histone H3 (pH3) immunostaining was used to assess late G2 and M-phase entry (Hendzel et al., 1997), wherein the proportion of neurons positive for foci (late G2) or pan-nuclear (M-phase) staining out of all MAP2 positive transfected neurons was calculated in each of 3 independent experiments in each treatment condition**.** Cell counting in BrdU, active Caspase-3, pH3 and γ-H2AX experiments was done with 20x (Zoom, 1.5) or 40x objectives with AF 6500-7000 fluorescence microscope (Leica) and a DU8285 VP-4324 camera (Andor). Confocal microscope images were acquired with 40x or 63x objectives using upright or inverted TCS SP5 confocal microscopes (Leica). For 3D image reconstructions, images were taken with a 63x objective with 1.7- to 3.6-times zoom, in 50 to 69 z-stacks of 0.13 to 0.25 µm step-sizes. 3D reconstructions and rotating 3D movies were generated using Icy bioimage informatics platform (de Chaumont et al., 2012).

Live imaging of neuronal cell-cycle

Neurons were cultured as described above in µ-Dish 35mm, high Grid-500 cell culture dishes with ibidi polymer coverslip bottom (Ibidi) coated with 0.5 mg/ml polyornithine (Sigma-Aldrich). Live neuronal imaging was performed in a sealed chamber at 37ºC

and 5 % CO_2 with 20x objective of a AF 6500-7000 fluorescence microscope and recorded with DU8285 VP-4324 camera. Pictures and Movies were generated using Leica Application Suite X (Leica). Time intervals between pictures and experiments duration are described in each movie. For cell counting studies of anaphase and cytokinesis, neurons were identified by morphological criteria based on RFP signal. When in doubt, cells were either not included in the quantification or neuronal identity confirmed by MAP2 immunostaining and included in the quantification. Binucleated neurons were not quantified. Neurons that presented obvious signs of cell-death during the first hour of recording were not included in the quantification. Chromosome segregation during anaphase was identified by H2B-GFP (Kanda et al., 1998) and cleavage furrow ingression by RFP.

Measurement of the AIS

AnkyrinG (AnkG) was used to evaluate changes in the AIS of neurons at different stages of the cell-cycle. All groups were treated with Wee1 inhibitor MK1775 (Hirai et al., 2009) (900 nM) to abrogate the G2 checkpoint and with the Mps1 inhibitor AZ3146 (Hewitt et al., 2010) (10 µM) 2.5 h later to abrogate the SAC. Neurons in the interphase, prophase and prometaphase to telophase groups were fixed 3 h after G2 checkpoint abrogation. Stages in between prometaphase and telophase could not be reliably distinguished by nuclear morphology and were thus grouped together. Multinucleated neurons were used to assess premature M-phase exit and were fixed 6 and 9 h after G2 checkpoint abrogation. Multinucleated neurons still presenting mitotic chromatin condensation or evidence of pyknosis were not included in the quantification. Neurons in all of the aforementioned groups co-expressed t1EK2/p53DN/TOP2α/RFP. Control neurons expressing LacZ/p53DN/TOP2α/RFP were fixed 9 h after G2 checkpoint

abrogation. Images were acquired on an upright Leica SP5 confocal microscope with a 63× objective, 1024 × 1024 pixels in z stacks with 0.5-µm steps and a Z-projection was obtained. Measurements of AnkG fluorescence intensity were performed by Fiji-ImageJ software. We drew a line starting at the limit of neuronal soma identified by MAP2 staining, and extended it along the AnkG staining or the RFP signal of the axon. Data were obtained after background subtraction. Then, data were smoothed every 1 µm using Sigma Plot 12.5 software. AIS start and end positions were obtained following the criteria described previously (Grubb and Burrone, 2010). Then total fluorescence intensity for each AIS was obtained. Total fluorescent intensity was then divided by the length of the AIS to obtain the mean AnkG fluorescence per 1 µm (AnkG/µm). To avoid variability between cell cultures and treatment exposure times, we normalized the mean AnkG/µm of transfected neurons to the nearest neighboring non-transfected neurons in the same image.

Statistical Analysis

Statistical analysis was performed using SPSS (version 24.0). Statistical analysis of BrdU time course experiments were done with Chi-square test of independence and Bonferroni corrected post-hoc multiple comparisons ($\alpha = 0.05$, two-tailed). Expected counts were more than 5 in all cells. Analysis of active-Caspase-3 and γ-H2AX experiments were done with Fisher's exact test ($\alpha = 0.05$, two-tailed). For AnkG/µm in AIS experiments, outliers were identified by boxplots. Normality was assessed with Shapiro-Wilk test of normality and Normal Q-Q Plots. Homogeneity of variances with Levene's test for equality of variances. Omnibus testing was performed with Welch's F test and post-hoc multiple comparisons with the Games-Howell method ($\alpha = 0.05$, two-

tailed). Quantitative data are expressed as mean ± standard error of the mean (s.e.m.). Significance was $p<0.05$ (*), $p<0.01$ (**), and $p<0.001$ (***).

ACKNOWLEDGMENTS

We thank Stuart Wilson, William Kaelin, Geoff Wahl, and Corrado Santocanale for the plasmids used in this study, and S. Casas-Tintó, and F. Wandosell for the critical reading of the manuscript. We also thank the Department of Statistics of SGAI-CSIC. Funding: The study was supported by Ministerio de Economía y Competitividad grant SAF2015-68488-R (J.M.F.), SAF2015-65315-R (J.J.G.), and Ministerio de Educación, Cultura y Deporte grant FPU1305084 (C.C.W.).

AUTHOR CONTRIBUTIONS

C.C.W., J.M.F., and J.J.G. conceived the study, C.C.W. performed the experiments and analyzed data, W.Z. analyzed data, I.P.-P. analyzed data, E.B.-A. provided expertise and feedback, C.C.W. and J.M.F. wrote the manuscript.

COMPETING FINANTIAL INTERESTS

The authors declare no competing financial interests.

REFERENCES

- Absalon, S., Kochanek, D.M., Raghavan, V. and Krichevsky, A.M., 2013. MiR-26b, upregulated in Alzheimer's disease, activates cell cycle entry, tau-phosphorylation, and apoptosis in postmitotic neurons. *J. Neurosci.*, **33**(37), pp.14645-14659.
- Ajioka, I., Martins, R.A., Bayazitov, I.T., Donovan, S., Johnson, D.A., Frase, S., Cicero, S.A., Boyd, K., Zakharenko, S.S. and Dyer, M.A., 2007. Differentiated

horizontal interneurons clonally expand to form metastatic retinoblastoma in mice. *Cell*, **131**(2), pp.378-390.

- Akli, S., Van Pelt, C.S., Bui, T., Multani, A.S., Chang, S., Johnson, D., Tucker, S. and Keyomarsi, K., 2007. Overexpression of the low molecular weight cyclin E in transgenic mice induces metastatic mammary carcinomas through the disruption of the ARF-p53 pathway. *Cancer Res*, **67**(15), pp.7212-7222.
- Al-Ubaidi, M.R., Hollyfield, J.G., Overbeek, P.A. and Baehr, W., 1992. Photoreceptor degeneration induced by the expression of simian virus 40 large tumor antigen in the retina of transgenic mice. *Proc. Natl. Acad. Sci. USA*, **89**(4), pp.1194-1198.
- Anda, F.C., Madabhushi, R., Rei, D., Meng, J., Gräff, J., Durak, O., Meletis, K., Richter, M., Schwanke, B., Mungenast, A., et al. 2016. Cortical neurons gradually attain a post-mitotic state. *Cell Res.*, **26**(9), p.1033-1047.
- Arendt, T., Brückner, M.K., Mosch, B. and Lösche, A., 2010. Selective cell death of hyperploid neurons in Alzheimer's disease. *Am. J. Pathol.*, **177**(1), pp.15-20.
- Bagheri-Yarmand, R., Biernacka, A., Hunt, K.K. and Keyomarsi, K., 2010. Low molecular weight cyclin E overexpression shortens mitosis, leading to chromosome missegregation and centrosome amplification. *Cancer Res.*, **70**(12), pp.5074-5084.
- Bartkova, J., Hořejší, Z., Koed, K., Krämer, A., Tort, F., Zieger, K., Guldberg, P., Sehested, M., Nesland, J.M., Lukas, C., et al., 2005. DNA damage response as a candidate anti-cancer barrier in early human tumorigenesis. *Nature*, **434**(7035), p.864-870.
- Bartkova, J., Rezaei, N., Liontos, M., Karakaidos, P., Kletsas, D., Issaeva, N., Vassiliou, L.V.F., Kolettas, E., Niforou, K., Zoumpourlis, V.C., et al. 2006.

Oncogene-induced senescence is part of the tumorigenesis barrier imposed by DNA damage checkpoints. *Nature*, **444**(7119), p.633-637.

- Bester, A.C., Roniger, M., Oren, Y.S., Im, M.M., Sarni, D., Chaoat, M., Bensimon, A., Zamir, G., Shewach, D.S. and Kerem, B., 2011. Nucleotide deficiency promotes genomic instability in early stages of cancer development. *Cell*, **145**(3), pp.435-446.
- Brito, D.A. and Rieder, C.L., 2006. Mitotic checkpoint slippage in humans occurs via cyclin B destruction in the presence of an active checkpoint. *Curr. Biol.*, **16**(12), pp.1194-1200.
- Chatterjee, N., Sanphui, P., Kemeny, S., Greene, L.A. and Biswas, S.C., 2016. Role and regulation of Cdc25A phosphatase in neuron death induced by NGF deprivation or β-amyloid. *Cell Death Discov.* **2**, p.16083.
- Chen, D., Livne-bar, I., Vanderluit, J.L., Slack, R.S., Agochiya, M. and Bremner, R., 2004. Cell-specific effects of RB or RB/p107 loss on retinal development implicate an intrinsically death-resistant cell-of-origin in retinoblastoma. *Cancer Cell*, ***5***(6), pp.539-551.
- Chen, T., Sun, Y., Ji, P., Kopetz, S. and Zhang, W., 2015. Topoisomerase IIα in chromosome instability and personalized cancer therapy. *Oncogene*, **34**(31), p.4019-4031.
- Chin, L.S., Li, L., Ferreira, A., Kosik, K.S. and Greengard, P., 1995. Impairment of axonal development and of synaptogenesis in hippocampal neurons of synapsin I-deficient mice. *Proc. Natl. Acad. Sci. USA*, **92**(20), pp.9230-9234.
- Cicero, S. and Herrup, K., 2005. Cyclin-dependent kinase 5 is essential for neuronal cell cycle arrest and differentiation. *J. Neurosci.*, **25**(42), pp.9658-9668.

- Copani, A., Condorelli, F., Caruso, A., Vancheri, C., Sala, A., Stella, A.G., Canonico, P.L., Nicoletti, F. and Sortino, M.A., 1999. Mitotic signaling by β-amyloid causes neuronal death. *FASEB J.*, **13**(15), pp.2225-2234.
- Coppé, J.P., Desprez, P.Y., Krtolica, A. and Campisi, J., 2010. The senescence-associated secretory phenotype: the dark side of tumor suppression. *Ann. Rev. Pathol.*, **5**, pp.99-118.
- Das, R.M., Van Hateren, N.J., Howell, G.R., Farrell, E.R., Bangs, F.K., Porteous, V.C., Manning, E.M., McGrew, M.J., Ohyama, K., Sacco, M.A., et al. 2006. A robust system for RNA interference in the chicken using a modified microRNA operon. *Dev. Biol.*, **294**(2), pp.554-563.
- de Chaumont, F., Dallongeville, S., Chenouard, N., Hervé, N., Pop, S., Provoost, T., Meas-Yedid, V., Pankajakshan, P., Lecomte, T., Le Montagner, Y., et al. 2012. Icy: an open bioimage informatics platform for extended reproducible research. *Nat. Methods*, **9**(7), p.690-696.
- Feddersen, R.M., Ehlenfeldt, R., Yunis, W.S., Clark, H.B. and Orr, H.T., 1992. Disrupted cerebellar cortical development and progressive degeneration of Purkinje cells in SV40 T antigen transgenic mice. *Neuron*, **9**(5), pp.955-966.
- Ferguson, K.L., Vanderluit, J.L., Hébert, J.M., McIntosh, W.C., Tibbo, E., MacLaurin, J.G., Park, D.S., Wallace, V.A., Vooijs, M., McConnell, S.K. and Slack, R.S., 2002. Telencephalon-specific Rb knockouts reveal enhanced neurogenesis, survival and abnormal cortical development. *EMBO J.*, ***21***(13), pp.3337-3346.
- Fielder, E., von Zglinicki, T. and Jurk, D., 2017. The DNA damage response in neurons: die by apoptosis or survive in a senescence-like state? *J. Alzheimers Dis.*, **60**(s1), pp.S107-S131.

- Frade, J.M. and Ovejero-Benito, M.C., 2015. Neuronal cell cycle: the neuron itself and its circumstances. *Cell Cycle*, **14**(5), pp.712-720.
- Fragkos, M. and Naim, V., 2017. Rescue from replication stress during mitosis. *Cell Cycle*, **16**(7), pp.613-633.
- Friedmann-Morvinski, D., Bushong, E.A., Ke, E., Soda, Y., Marumoto, T., Singer, O., Ellisman, M.H. and Verma, I.M., 2012. Dedifferentiation of neurons and astrocytes by oncogenes can induce gliomas in mice. *Science*, **338**(6110), pp.1080-1084.
- Geng, Y., Yu, Q., Sicinska, E., Das, M., Schneider, J.E., Bhattacharya, S., Rideout, W.M., Bronson, R.T., Gardner, H. and Sicinski, P., 2003. Cyclin E ablation in the mouse. *Cell*, **114**(4), pp.431-443.
- Greene, L.A., Liu, D.X., Troy, C.M. and Biswas, S.C., 2007. Cell cycle molecules define a pathway required for neuron death in development and disease. *Biochim. Biophys. Acta.* **1772**(4), pp.392-401.
- Grubb, M.S. and Burrone, J., 2010. Activity-dependent relocation of the axon initial segment fine-tunes neuronal excitability. *Nature*, **465**(7301), p.1070-1074.
- Halazonetis, T.D., Gorgoulis, V.G. and Bartek, J., 2008. An oncogene-induced DNA damage model for cancer development. *Science*, **319**(5868), pp.1352-1355.
- Harbison, R.A., Ryan, K.R., Wilkins, H.M., Schroeder, E.K., Loucks, F.A., Bouchard, R.J. and Linseman, D.A., 2011. Calpain plays a central role in 1-methyl-4-phenylpyridinium (MPP^+)-induced neurotoxicity in cerebellar granule neurons. *Neurotox. Res.*, **19**(3), pp.374-388.
- Hendzel, M.J., Wei, Y., Mancini, M.A., Van Hooser, A., Ranalli, T., Brinkley, B.R., Bazett-Jones, D.P. and Allis, C.D., 1997. Mitosis-specific phosphorylation of histone H3 initiates primarily within pericentromeric heterochromatin during G2

and spreads in an ordered fashion coincident with mitotic chromosome condensation. *Chromosoma*, **106**(6), pp.348-360.

- Herrup, K. and Yang, Y., 2007. Cell cycle regulation in the postmitotic neuron: oxymoron or new biology? *Nat. Rev. Neurosci.*, **8**(5), p.368-378.
- Hewitt, L., Tighe, A., Santaguida, S., White, A.M., Jones, C.D., Musacchio, A., Green, S. and Taylor, S.S., 2010. Sustained Mps1 activity is required in mitosis to recruit O-Mad2 to the Mad1–C-Mad2 core complex. *J. Cell Biology*, **190**(1), pp.25-34.
- Hirai, H., Iwasawa, Y., Okada, M., Arai, T., Nishibata, T., Kobayashi, M., Kimura, T., Kaneko, N., Ohtani, J., Yamanaka, K., et al. 2009. Small-molecule inhibition of Wee1 kinase by MK-1775 selectively sensitizes p53-deficient tumor cells to DNA-damaging agents. *Mol. Cancer Ther.*, **8**(11), pp.2992-3000.
- Hoozemans, J.J., Brückner, M.K., Rozemuller, A.J., Veerhuis, R., Eikelenboom, P. and Arendt, T., 2002. Cyclin D1 and cyclin E are co-localized with cyclo-oxygenase 2 (COX-2) in pyramidal neurons in Alzheimer disease temporal cortex. *J. Neuropathol. Exp. Neurol.*, **61**(8), pp.678-688.
- Irwin, M., Marin, M.C., Phillips, A.C., Seelan, R.S., Smith, D.I., Liu, W., Flores, E.R., Tsai, K.Y., Jacks, T., Vousden, K.H. and Kaelin Jr, W.G., 2000. Role for the p53 homologue p73 in E2F-1-induced apoptosis. *Nature*, **407**(6804), p.645-648.
- Jahn, S.C., Law, M.E., Corsino, P.E., Rowe, T.C., Davis, B.J. and Law, B.K., 2013. Assembly, activation, and substrate specificity of cyclin D1/Cdk2 complexes. *Biochemistry*, **52**(20), pp.3489-3501.
- Jones, R.M., Mortusewicz, O., Afzal, I., Lorvellec, M., Garcia, P., Helleday, T. and Petermann, E., 2013. Increased replication initiation and conflicts with transcription underlie Cyclin E-induced replication stress. *Oncogene*, **32**(32), p.3744-3753.

- Kanda, T., Sullivan, K.F. and Wahl, G.M., 1998. Histone–GFP fusion protein enables sensitive analysis of chromosome dynamics in living mammalian cells. *Curr. Biol.*, **8**(7), pp.377-385.
- Kaufman, M.H., 1992. *The atlas of mouse development*. London: Academic press.
- Kinner, A., Wu, W., Staudt, C. and Iliakis, G., 2008. γ-H2AX in recognition and signaling of DNA double-strand breaks in the context of chromatin. *Nucl. Acids Res.*, **36**(17), pp.5678-5694.
- Kruman, I.I., Wersto, R.P., Cardozo-Pelaez, F., Smilenov, L., Chan, S.L., Chrest, F.J., Emokpae Jr, R., Gorospe, M. and Mattson, M.P., 2004. Cell cycle activation linked to neuronal cell death initiated by DNA damage. *Neuron*, **41**(4), pp.549-561.
- Konishi, Y., Lehtinen, M., Donovan, N., and Bonni, A., 2002. Cdc2 phosphorylation of BAD links the cell cycle to the cell death machinery. *Mol. Cell.* **9**(5), pp.1005-1016.
- Kuan, C.Y., Schloemer, A.J., Lu, A., Burns, K.A., Weng, W.L., Williams, M.T., Strauss, K.I., Vorhees, C.V., Flavell, R.A., Davis, R.J. and Sharp, F.R., 2004. Hypoxia-ischemia induces DNA synthesis without cell proliferation in dying neurons in adult rodent brain. *J. Neurosci.*, **24**(47), pp.10763-10772.
- Lan, W. and Cleveland, D.W., 2010. A chemical tool box defines mitotic and interphase roles for Mps1 kinase. *J. Cell Biol.*, **190**(1), pp.21-24.
- Lee, K.H., Lee, S.J., Lee, H.J., Choi, G.E., Jung, Y.H., Kim, D.I., Gabr, A.A., Ryu, J.M. and Han, H.J., 2017. Amyloid β1-42 (Aβ1-42) induces the CDK2-mediated phosphorylation of Tau through the activation of the mTORC1 signaling pathway while promoting neuronal cell death. *Front. Mol. Neurosci.*, **10**, p.229

- Lopes, J.P., Oliveira, C.R. and Agostinho, P., 2009. Cdk5 acts as a mediator of neuronal cell cycle re-entry triggered by amyloid-β and prion peptides. *Cell Cycle*, **8**(1), pp.97-104.
- Manic, G., Obrist, F., Sistigu, A. and Vitale, I., 2015. Trial watch: targeting ATM–CHK2 and ATR–CHK1 pathways for anticancer therapy. *Mol. Cell. Oncol.*, **2**(4), p.e1012976.
- Mayer, T.U., Kapoor, T.M., Haggarty, S.J., King, R.W., Schreiber, S.L. and Mitchison, T.J., 1999. Small molecule inhibitor of mitotic spindle bipolarity identified in a phenotype-based screen. *Science*, **286**(5441), pp.971-974.
- Mazumder, S., Plesca, D. and Almasan, A., 2008. Caspase-3 activation is a critical determinant of genotoxic stress-induced apoptosis. *Methods Mol. Biol.* **414**, 13-21.
- Minella, A.C., Swanger, J., Bryant, E., Welcker, M., Hwang, H. and Clurman, B.E., 2002. p53 and p21 form an inducible barrier that protects cells against cyclin E-cdk2 deregulation. *Curr. Biol.*, **12**(21), pp.1817-1827.
- Musacchio, A., and Salmon, E.D., 2007. The spindle-assembly checkpoint in space and time. *Nat. Rev. Mol. Cell Biol*. **8**(5), 379–393.
- Nagy, Z., Esiri, M.M., Cato, A.M. and Smith, A.D., 1997. Cell cycle markers in the hippocampus in Alzheimer's disease. *Acta Neuropathol.*, **94(**1), pp.6-15.
- Neelsen, K.J., Zanini, I.M., Herrador, R. and Lopes, M., 2013. Oncogenes induce genotoxic stress by mitotic processing of unusual replication intermediates. *J Cell Biol*, **200**(6), pp.699-708.
- Odajima, J., Wills, Z.P., Ndassa, Y.M., Terunuma, M., Kretschmannova, K., Deeb, T.Z., Geng, Y., Gawrzak, S., Quadros, I.M., Newman, J., et al. 2011. Cyclin E constrains Cdk5 activity to regulate synaptic plasticity and memory formation. *Dev. Cell*, **21**(4), pp.655-668.

- Oshikawa, M., Okada, K., Nakajima, K. and Ajioka, I., 2013. Cortical excitatory neurons become protected from cell division during neurogenesis in an Rb family-dependent manner. *Development*, **140**(11), pp.2310-2320.
- Oshikawa, M., Okada, K., Tabata, H., Nagata, K.I. and Ajioka, I., 2017. Dnmt1-dependent Chk1 pathway suppression is protective against neuron division. *Development*, **144**(18), pp.3303-3314.
- Piekny, A.J. and Maddox, A.S., 2010. The myriad roles of Anillin during cytokinesis. *Semin. Cell Dev. Biol.* **21**(9), 881-891.
- Porter, D.C., Zhang, N., Danes, C., McGahren, M.J., Harwell, R.M., Faruki, S. and Keyomarsi, K., 2001. Tumor-specific proteolytic processing of cyclin E generates hyperactive lower-molecular-weight forms. *Mol. Cell. Biol.*, **21**(18), pp.6254-6269.
- Rasband, M.N., 2010. The axon initial segment and the maintenance of neuronal polarity. *Nat. Rev. Neurosci.*, **11**(8), p.552-562.
- Ray, J., Peterson, D.A., Schinstine, M. and Gage, F.H., 1993. Proliferation, differentiation, and long-term culture of primary hippocampal neurons. *Proc. Natl. Acad. Sci. USA*, **90**(8), pp.3602-3606.
- Sarkaria, J.N., Busby, E.C., Tibbetts, R.S., Roos, P., Taya, Y., Karnitz, L.M. and Abraham, R.T., 1999. Inhibition of ATM and ATR kinase activities by the radiosensitizing agent, caffeine. *Cancer Res.*, **59**(17), pp.4375-4382.
- Schafer, D.P., Jha, S., Liu, F., Akella, T., McCullough, L.D. and Rasband, M.N., 2009. Disruption of the axon initial segment cytoskeleton is a new mechanism for neuronal injury. *J. Neurosci.*, **29**(42), pp.13242-13254.
- Schmetsdorf, S., Arnold, E., Holzer, M., Arendt, T. and Gärtner, U., 2009. A putative role for cell cycle-related proteins in microtubule-based neuroplasticity. *Eur. J. Neurosci.*, **29**(6), pp.1096-1107.

- Schwartz, E.I., Smilenov, L.B., Price, M.A., Osredkar, T., Baker, R.A., Ghosh, S., Shi, F.D., Vollmer, T.L., Lencinas, A., Stearns, D.M., et al. 2007. Cell cycle activation in postmitotic neurons is essential for DNA repair. *Cell Cycle*, **6**(3), pp.318-329.
- Siu, K.T., Rosner, M.R. and Minella, A.C., 2012. An integrated view of cyclin E function and regulation. *Cell Cycle*, **11**(1), pp.57-64.
- Skoufias, D.A., Lacroix, F.B., Andreassen, P.R., Wilson, L. and Margolis, R.L., 2004. Inhibition of DNA decatenation, but not DNA damage, arrests cells at metaphase. *Mol. Cell*, **15**(6), pp.977-990.
- Smith, A.P., Henze, M., Lee, J.A., Osborn, K.G., Keck, J.M., Tedesco, D., Bortner, D.M., Rosenberg, M.P. and Reed, S.I., 2006. Deregulated cyclin E promotes p53 loss of heterozygosity and tumorigenesis in the mouse mammary gland. *Oncogene*, **25**(55), p.7245-7259.
- Staropoli, J.F., McDermott, C., Martinat, C., Schulman, B., Demireva, E. and Abeliovich, A., 2003. Parkin is a component of an SCF-like ubiquitin ligase complex and protects postmitotic neurons from kainate excitotoxicity. *Neuron*, **37**(5), pp.735-749.
- Su, S.C. and Tsai, L.H., 2011. Cyclin-dependent kinases in brain development and disease. *Annu. Rev. Cell Dev. Biol.*, **27**, pp.465-491.
- Teixeira, L.K. and Reed, S.I., 2017. Cyclin E Deregulation and Genomic Instability. *Adv. Exp. Med. Biol.*, **1042**, pp.527-547.
- Vassilev, L.T., Tovar, C., Chen, S., Knezevic, D., Zhao, X., Sun, H., Heimbrook, D.C. and Chen, L., 2006. Selective small-molecule inhibitor reveals critical mitotic functions of human CDK1. *Proc. Natl. Acad. Sci. USA*, **103**(28), pp.10660-10665.

- Veas-Pérez de Tudela, M., Maestre, C., Delgado-Esteban, M., Bolaños, J.P. and Almeida, A., 2015. Cdk5-mediated inhibition of APC/C-Cdh1 switches on the cyclin D1-Cdk4-pRb pathway causing aberrant S-phase entry of postmitotic neurons. *Sci. Rep.*, **5**, p.18180.
- Verdaguer, E., García-Jordà, E., Canudas, A.M., Domínguez, E., Jiménez, A., Pubill, D., Escubedo, E., Pallàs, J.C.M. and Camins, A., 2002. Kainic acid-induced apoptosis in cerebellar granule neurons: an attempt at cell cycle re-entry. *Neuroreport*, **13**(4), pp.413-416.
- Vitale, I., Galluzzi, L., Castedo, M. and Kroemer, G., 2011. Mitotic catastrophe: a mechanism for avoiding genomic instability. *Nat. Rev. Mol. Cell Biol.*, **12**(6), p.385-392.
- Wu, K.Z., Wang, G.N., Fitzgerald, J., Quachthithu, H., Rainey, M.D., Cattaneo, A., Bachi, A. and Santocanale, C., 2016. DDK dependent regulation of TOP2A at centromeres revealed by a chemical genetics approach. *Nucleic Acids Res.*, **44**(18), pp.8786-8798.
- Xu, X.L., Singh, H.P., Wang, L., Qi, D.L., Poulos, B.K., Abramson, D.H., Jhanwar, S.C. and Cobrinik, D., 2014. Rb suppresses human cone-precursor-derived retinoblastoma tumours. *Nature*, ***514***(7522), p.385-388.
- Yang, Y., Geldmacher, D.S. and Herrup, K., 2001. DNA replication precedes neuronal cell death in Alzheimer's disease. *J. Neurosci.*, **21**(8), pp.2661-2668.
- Zhu, X., Siedlak, S.L., Wang, Y., Perry, G., Castellani, R.J., Cohen, M.L. and Smith, M.A., 2008. Neuronal binucleation in Alzheimer disease hippocampus. *Neuropathol. Appl. Neurobiol.*, **34**(4), pp.457-465.

- Zindy, F., Cunningham, J.J., Sherr, C.J., Jogal, S., Smeyne, R.J. and Roussel, M.F., 1999. Postnatal neuronal proliferation in mice lacking Ink4d and Kip1 inhibitors of cyclin-dependent kinases. *Proc. Natl. Acad. Sci. USA* **96**(23), pp.13462-13467.